Silicon Photonics Design, Fabrication and Data Analysis manuscript No.
(will be inserted by the editor)

Design Proposal: Mach-Zehnder Interferometer, ring resonator and fiber Bragg grating.

Julio Souto Garnelo

04/03/2025

Abstract

1 Introduction

Since the beginning of the century, interest in silicon as the material of choice in photonic circuits has rapidly increased. Its compatibility with CMOS fabrication processes allows for highly scalable and low-cost circuits [5]. On top of that, it offers great optical properties, such as high optical confinement and the presence of non-linear interactions. As a result, silicon has established itself as the leading material for photonic integrated circuits.

The objective of this work is to highlight silicon for the construction of photonic circuits, with a special focus on Mach-Zehnder interferometers, ring resonators, and fiber Bragg gratings. Using several architectures, we will perform a comparison between the theoretical and experimental results, which will be obtained after fabrication, via electron beam lithography, and testing.

Mach-Zehnder interferometers are of great importance in the field of photonics as they can be used as optical switches, filters, or modulators [6]. These devices are building blocks for optical circuits thanks to their dynamic response to differences in path length and material properties between the interferometer's arms.

Ring resonators and fiber Bragg gratings are also commonly used photonic components that are included in our designs. The first ones display resonance with certain wavelengths, making them good narrow-bandpass filters [7]. The last one presents constructive interference due to reflection for a certain wavelength that satisfies Bragg's condition, which allows for their use in sensing and filtering [8].

Address(es) of author(s) should be given

2 Theory

For the purpose of performing a theoretical and experimental analysis of our constructed structures, we will first delve into the behavior of each of the components of our Mach-Zehnder interferometers.

We will commence with the Y-Branches, an optical component with three branches that can act as a splitter or a combiner. In the case of the interferometer we make use of a splitter and a combiner, each near a grating coupler. The splitter will divide optical input into the two branches of the interferometer.

$$I_{1,2} = \frac{I_i}{2}, E_{1,2} = \frac{E_i}{\sqrt{2}} \tag{1}$$

Where $I_{1,2}$ and $E_{1,2}$ are the output power and electric field, respectively. Then, each branch of the interferometer can vary in length, refractive index and attenuation coefficient. For our case scenario we will consider only length differences between arms. Finally, the combiner collects the light from both arms and combines them according to Equation 2.

$$E_o = \frac{E_1 + E_2}{\sqrt{2}} \tag{2}$$

In order to characterize the MZI we need to consider how light propagates in the waveguides. From Maxwell's equations we write the propagation of an electric field in a medium.

$$E = E_0 e^{i(\omega t - \beta z)} \tag{3}$$

Where the factor β is dependent on the medium, via the refractive index, and the wavelength.

$$\beta = \frac{2\pi n}{\lambda} \tag{4}$$

Thus, by applying the effect of the splitter and combiner we find the expression of the electric field at the output of the interferometer.

$$E_{o1,o2} = \frac{E_i}{\sqrt{2}} e^{-i\beta L_{1,2} - \alpha L_{1,2}} \tag{5}$$

$$E_o = \frac{E_i}{2}(e^{-i\beta L_1 - \alpha L_1} + e^{-i\beta L_2 - \alpha L_2}) \tag{6}$$

Thus, from this final expression we can obtain that of the intensity, as it is squarely proportional to the electric field.

$$I_o = \frac{I_i}{4}|e^{-i\beta L_1 - \alpha L_1} + e^{-i\beta L_2 - \alpha L_2}|^2 \tag{7}$$

Simplifying by using Euler's formula we obtain a function with a cosine that varies according to the length differences between the interferometer's arms. This property is crucial, as it will allow the MZI to act as an optical switch. Nevertheless, when output power is zero it disperses in the medium as it does not disappear.

$$I_o = \frac{I_i}{2}[1 + cos(\beta \Delta L)] \tag{8}$$

We can then write the transfer function of the Mach Zehnder interferometer as a function of wavelength as seen in Equation 9.

$$T_{MZI}(\lambda) = \frac{1}{2}(1 + cos(\beta(\lambda)\Delta L) \tag{9}$$

Continuing with the characterization of the device, we can define the free spectral range, which corresponds to the spacing between consecutive peaks of the optical wave.

$$FSR(\lambda) = \Delta\lambda = \frac{\lambda^2}{\Delta L n_g} \tag{10}$$

Where n_g corresponds to the group index, the ratio of propagation of optical pulses in the medium. It takes into account dispersion, how the refractive index changes with wavelength.

$$n_g = n_{eff} - \lambda \frac{\partial n_{eff}}{\partial \lambda} \tag{11}$$

3 Modelling and Simulation

For our designs the waveguides used have been TE mode for 1550 nm wavelength and with dimensions of 500 μm width and standard height of 220 μm. The circuits were constructed using KLayout with the SiEpic EBeam package and modeled using Lumerical MODE solver and Lumerical INTERCONNECT.

Firstly, we modeled the mode profile, or intensity of the electric field, using the Lumerical MODE. This allowed us to observe the distribution of the first TE mode in the waveguide, as seen in Fig.1.

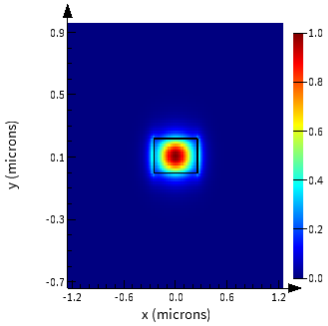

Fig. 1 Mode profile of waveguide, first TE mode. Lumerical FDE.

By performing frequency sweeps, we determined the evolution of the effective and group index with wavelength.

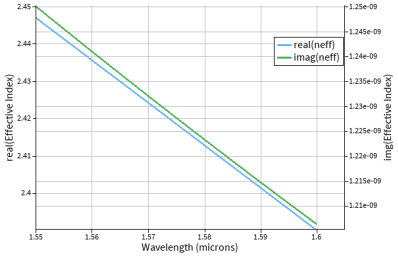

Fig. 2 Effective index as a function of wavelength.

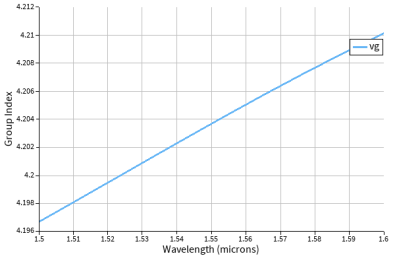

Fig. 3 Group index as a function of wavelength.

To describe the behavior of the effective refractive index we obtained the coefficients of the empirical formula of the compact model, which follows the general formula.

$$n_{eff}(\lambda) = n_1 - n_2(\lambda - \lambda_0) - n_3(\lambda - \lambda_0)^2 \tag{12}$$

Utilizing Lumerical FDE (MODE), we analyzed the waveguide by means of frequency sweeps from which we obtained the compact model of the waveguides used, which is displayed in Equation 13 and plotted in Fig.4.

$$n_{eff}(\lambda) = 2.4468 - 1.1334(\lambda - \lambda_0) - 0.04394(\lambda - \lambda_0)^2 \quad (13)$$

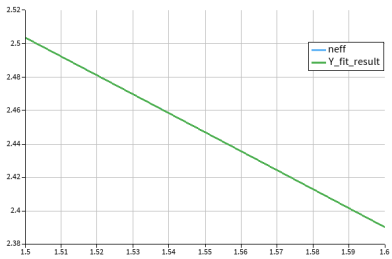

Fig. 4 Effective index as a function of wavelength using compact model.

Using the described components we proposed several Mach-Zehnder interferometers varying the difference in length between arms. For each we have calculated the theoretical free spectral range. Hereunder we gather the FSR for each ΔL in Table 1.

$\Delta L(\mu m)$	FSR $(\cdot 10^{-9})$
50	11.43
100	5.71
150	3.81
200	2.86
300	1.91

Table 1 Proposed path length differences and their corresponding theoretical free spectral ranges.

We have also characterized the transmission of the grating couplers and the Y-branches in order to observe their action individually.

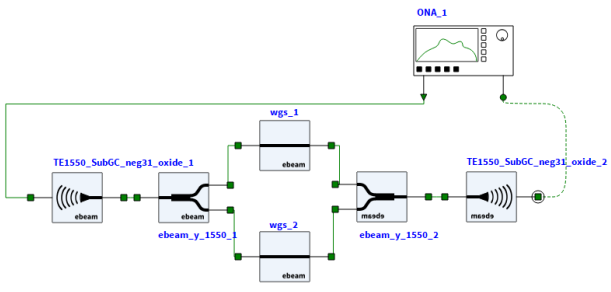

Fig. 5 Mach-Zehnder interferometer constructed in Lumerical INTERCONNECT with SiEpic EBeam components.

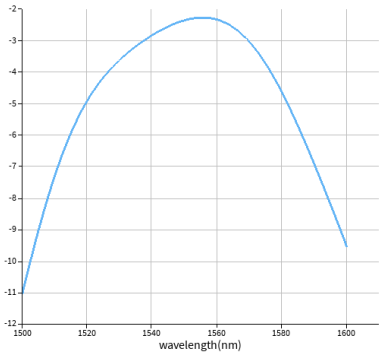

Fig. 6 Transfer of grating coupler in dB as a function of wavelength.

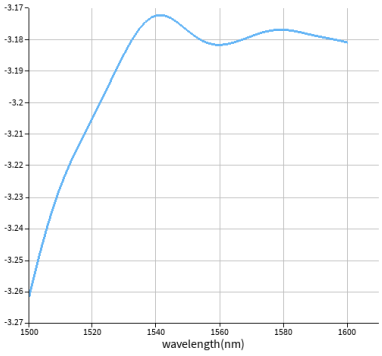

Fig. 7 Transfer of y-branch in dB as a function of wavelength..

Then, constructing the MZI circuit, we conducted a series of sweeps for each ΔL to compare with the experimental results.

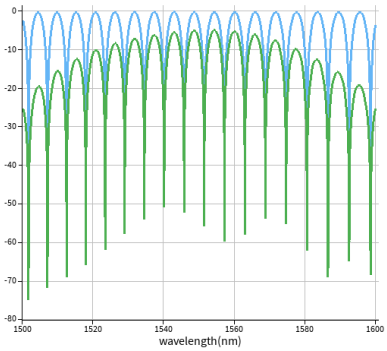

Fig. 8 Transfer of MZI with and without GC in dB as a function of wavelength.

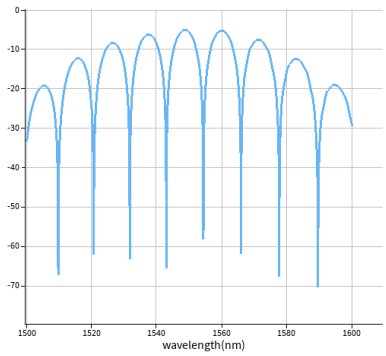

Fig. 9 Transfer of MZI with $\Delta L = 50\mu m$ in dB as a function of wavelength.

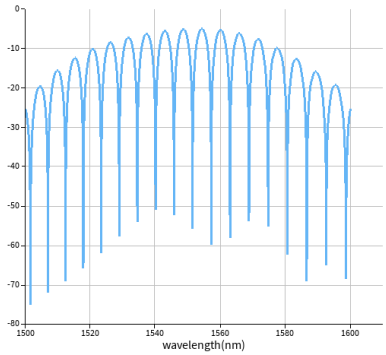

Fig. 10 Transfer of MZI with $\Delta L = 100\mu m$ in dB as a function of wavelength.

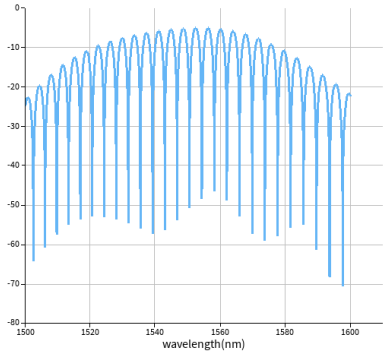

Fig. 11 Transfer of MZI with $\Delta L = 150\mu m$ in dB as a function of wavelength.

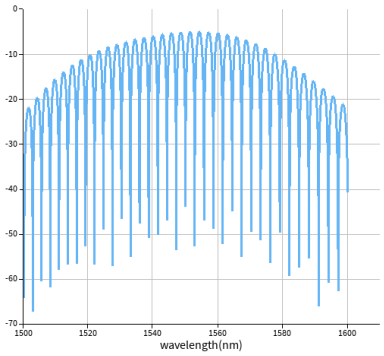

Fig. 12 Transfer of MZI with $\Delta L = 200\mu m$ in dB as a function of wavelength.

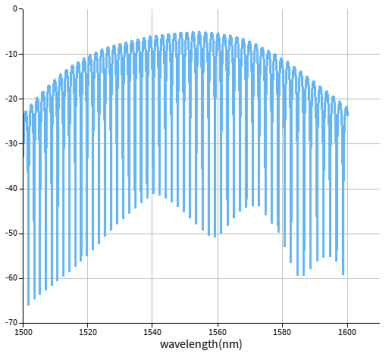

Fig. 13 Transfer of MZI with $\Delta L = 300\mu m$ in dB as a function of wavelength.

To further delve into the possibilities of silicon integrated photonics we have designed additional circuits to characterize the transmission of different configurations of ring couplers and a fiber Bragg grating.

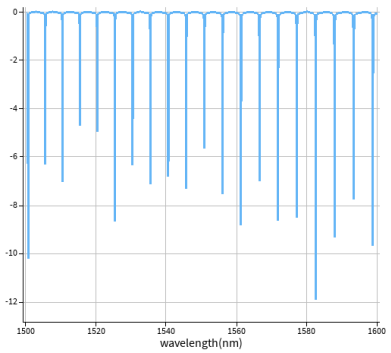

Fig. 14 Transfer of ring resonator with radius $25\mu m$ in dB as a function of wavelength.

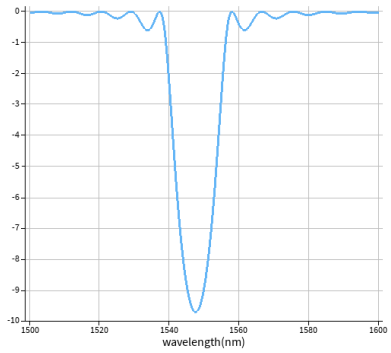

Fig. 15 Transfer of fiber Bragg grating in dB as a function of wavelength.

Finally, the draft layout contained several MZIs as well as a fiber Bragg grating and ring resonators.

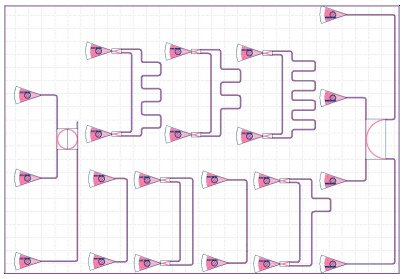

Fig. 16 Draft layout on KLayout using SiEpic EBeam components.

4 Fabrication

The photonic devices were fabricated using the NanoSOI MPW process provided by Applied Nanotools Inc. (Edmonton, Canada), which utilizes 100 keV electron beam lithography for direct-write patterning. The base material for fabrication consisted of silicon-on-insulator wafers with a 200 mm diameter, 220 nm device thickness, and 2 µm buffer oxide thickness. The wafer was pre-diced into 25x25 mm square substrates, with lines scribed on the backside to enable easy separation into smaller chips once the fabrication process was completed. The fabrication process began with an initial wafer clean using a piranha solution ($3:1 H2SO4:H2O2$) for 15 minutes, followed by a water/IPA rinse. Hydrogen silsesquioxane (HSQ) resist was then spin-coated onto the substrate and heated to evaporate the solvent.

Photonic device patterning was carried out using a JEOL JBX-8100FS electron beam instrument at The University of British Columbia. The exposure dosage was adjusted for proximity effects caused by electron backscatter from adjacent features. The shape writing order was optimized to minimize beam drift and improve patterning efficiency. After electron beam exposure and development with a tetramethylammonium sulfate (TMAH) solution, the devices were optically inspected for residues or defects. The chips were then mounted on a 4" handle wafer and underwent an anisotropic ICP-RIE etch process using chlorine, after confirming the etch rate. The resist was removed using a 10:1 buffer oxide wet etch, and the devices were inspected using a scanning electron microscope (SEM) to verify the patterning and etch quality. To finalize the process, a 2.2 µm oxide cladding was deposited using plasma-enhanced chemical vapor deposition (PECVD) based on tetraethyl orthosilicate (TEOS) at 300^{o}C. Throughout the process, reflectometry measurements were taken to verify the thicknesses of the device layer, buffer oxide, and cladding before the devices were delivered.

4.1 Manufacturing Challenges

During fabrication mismatches arise between the design and the result product. Thus, there is an inherent variability in the sizes of the different elements in the circuit. These can range between a certain range. In our case, we have established a certain range of 215.3 nm to 223.1 nm in height and 461.5 nm to 510 nm in width. Hereunder in Fig.17 and Fig.18 we can observe the dependence of the group and effective indexes on the wavelength for the different corners and nominal value (220 nm x 500 nm).

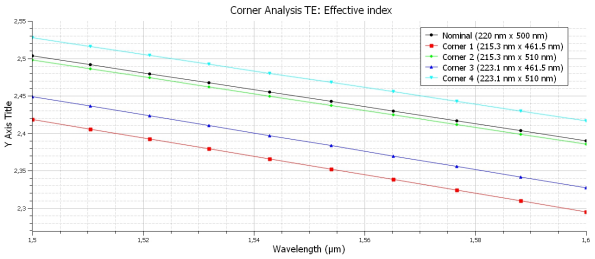

Fig. 17 Corner analysis for effective index, obtained using Lumerical MODE Frequency Sweeps.

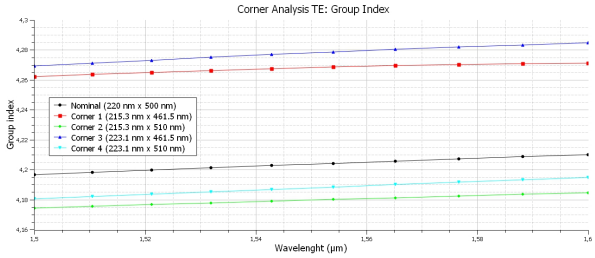

Fig. 18 Corner analysis for group index, obtained using Lumerical MODE Frequency Sweeps.

These are the ranges where our experimental results could lie as we have taken into account manufacturing challenges, therefore considering the inherent variability that the fabrication process entails.

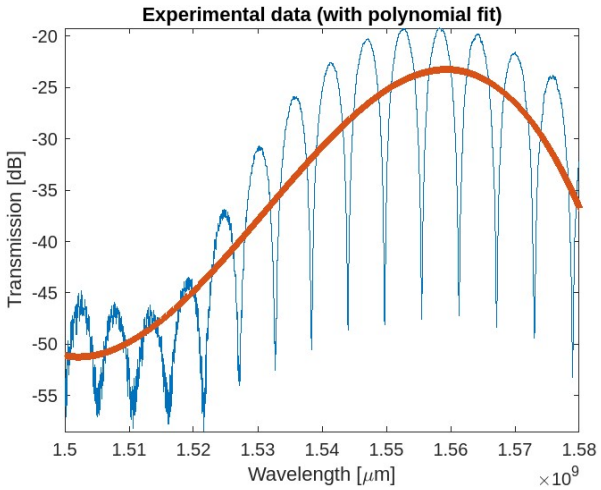

Fig. 19 Polynomial fitting (order 2) to MZI with $\Delta L = 50\mu m$.

5 Measurement Procedure

To characterize the devices, a custom-built automated test setup [1][11], controlled by automated software written in Python [9], was employed. The input source was an Agilent 81600B tunable laser, with Agilent 81635A optical power sensors used as output detectors. The wavelength was swept from 1500 to 1600 nm in 10 pm increments. A polarization-maintaining (PM) fiber was used to preserve the polarization state of the light and couple the TE polarization into the grating couplers [4]. A 90^{o} rotation was applied to inject light into the TM grating couplers [4]. A polarization-maintaining fiber array was employed to couple light in and out of the chip [10].

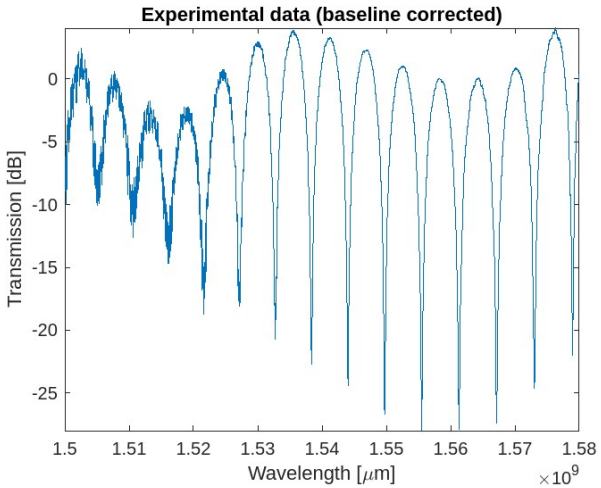

Fig. 20 Baseline corrected spectrum of MZI with $\Delta L = 50\mu m$.

6 Experimental Data and Analysis

After obtaining the experimental results, we have performed several adjustments in order to extract conclusions form our data. Firstly, we have carried our baseline correction to get rid of the contribution of the optical grating couplers to the spectrum. Then, by means of fitting a low order polynomial, we can substract this spectrum. As we can observe in Fig.19, this effectively flattens out our MZI spectrum.

Once our spectrums are corrected, we can obtain the experimental compact model parameters, the FSR and the group index for each spectrum. The results are gathered in Table 3. The fitting was performed by means of autocorrelation in MATLAB, and can be observed in Fig.21 and Fig.22. The rest of the fitting are in the annex. Nevertheless, it is worth to comment that some of the spectra did not behave properly when analysing the data, probably due to noise.

L (µm)	Simulated		Experimental	
	FSR (nm)	ng	FSR (nm)	ng
50	11.1341	4.3155	11.2575	4.2683
100	5.7346	4.1894	5.6275	4.2692
150	3.8475	4.1628	2.8841	5.5534
200	2.8325	4.2409	3.7136	4.1958
300	1.9008	4.2131	1.9216	8.3351

Table 2 Free spectral range and group index for proposed MZI configurations.

Most of the MZIs gave out comparable group indices and FSRs, except two, which can be attributed to poor fit, noise, and imprecision when finding the peaks. The fitting was performed with respect to the MZI tranfer function,

$$F = 10\log\left[\frac{1}{4}\left|1+\exp\left(i\frac{2\pi n_{\text{eff}}}{\lambda}\Delta L-\frac{\alpha\Delta L}{2}\right)\right|^2\right]+b \tag{14}$$

where we gave a certain starting point and the algorithm adjusted the parameters to fit to our spectra.

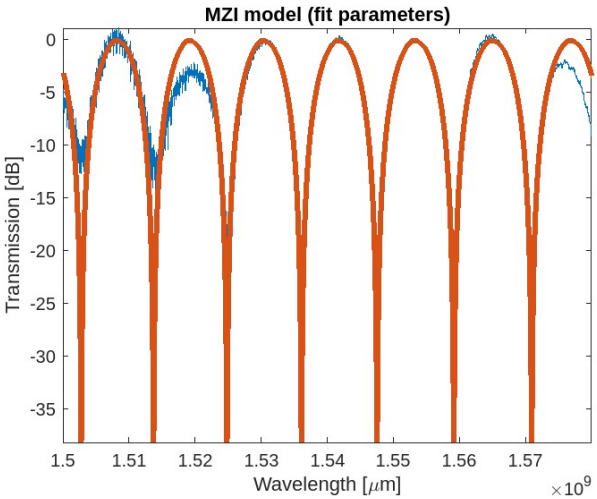

Fig. 21 Polynomial fitting of MZI with $\Delta L = 50\mu m$.

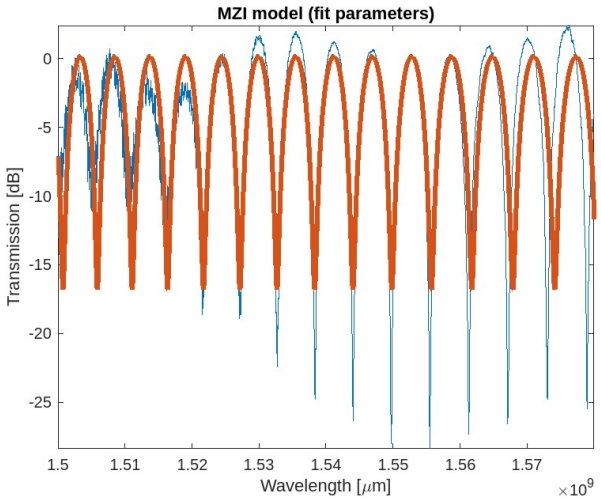

Fig. 22 Polynomial fitting of MZI with $\Delta L = 100\mu m$.

As a final comment, we want to include the raw data for a MZI, a ring resonator, and the Fiber Bragg Grating. As we can see in the following graphs, the spectrums correspond to what we expected plus the contribution of the grating coupler wavelength range.

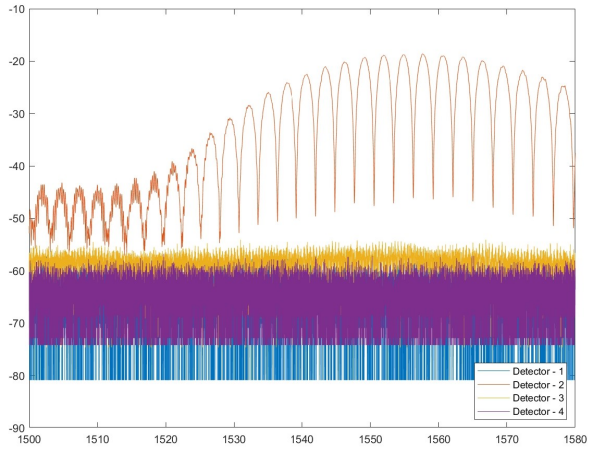

Fig. 23 Raw data of MZI with $\Delta L = 150\mu m$.

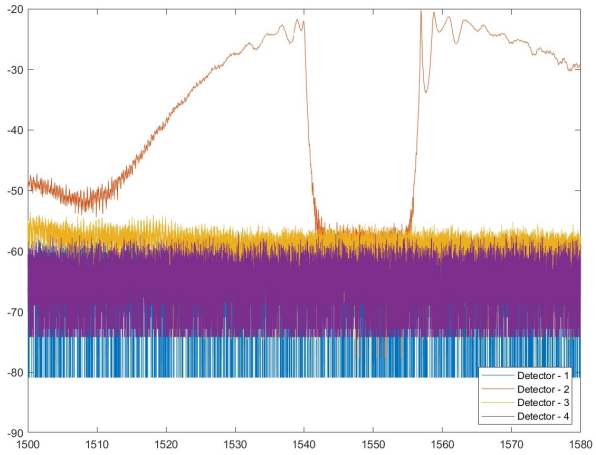

Fig. 24 Raw data of Fiber Bragg Grating.

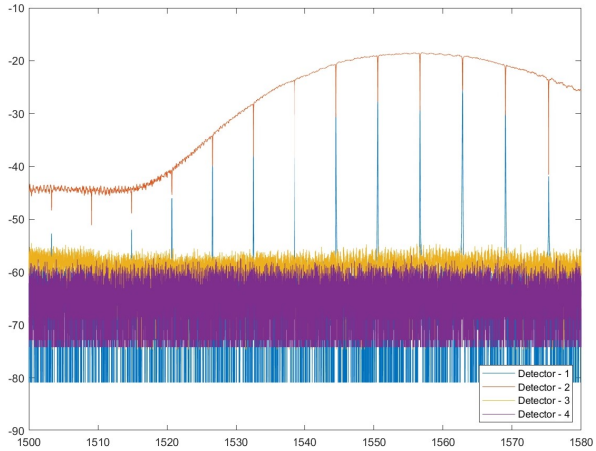

Fig. 25 Raw data of ring resonator with radius 25 μm.

7 Conclusion

In this report, we have analyzed the design, fabrication, and characterization of photonic integrated circuits, focusing mainly on Mach-Zehnder interferometers, although we have included as well ring resonators and fiber Bragg gratings. The goal of this work was to explore the potential of silicon photonics for creating efficient and scalable optical circuits using electron beam lithography for fabrication. The theoretical models, combined with simulation results, were used to predict the behavior of the devices, particularly the group index and the free spectral range (FSR).

Experimental results were obtained and analyzed, with a baseline correction process to account for discrepancies due to the grating couplers. The experimental data showed a high level of agreement with the theoretical TE models, where errors in the group index estimation were minimal.

The devices demonstrated good performance for the intended applications, such as optical switching and filtering, with the results for MZIs showing accurate FSR and group index values for most cases. Furthermore, the fabricated devices were successfully modeled and characterized, providing important insights into the behavior of waveguides with different dimensions and operating conditions. In conclusion, this work highlights the effectiveness of using silicon photonics for building high-performance PICs.

8 Acknowledgements

I acknowledge the edX UBCx Phot1x Silicon Photonics Design, Fabrication, and Data Analysis course, supported by the Natural Sciences and Engineering Research Council of Canada (NSERC) Silicon Electronic-Photonic Integrated Circuits (SiEPIC) Program. The devices were fabricated by Cameron Horvath at Applied Nanotools, Inc. Omid Esmaeeli performed the measurements at The University of British Columbia. I also acknowledge Lumerical Solutions, Inc., MathWorks, Mentor Graphics, Python, and KLayout for their contributions to the design software.

References

1. Chrostowski, L., Hochberg, M. (2015). Silicon Photonics Design. Cambridge University Press (CUP).
2. Bojko, R. J., Li, J., He, L., Baehr-Jones, T., Hochberg, M., Aida, Y. (2011). Electron beam lithography writing strategies for low loss, high confinement silicon optical waveguides. Journal of Vacuum Science Technology B, 29, 06F309. https://doi.org/10.1116/1.3653266
3. Chrostowski, L., Hochberg, M. (2015). Testing and packaging. In: Silicon Photonics Design. Cambridge University Press (CUP), pp. 381–405.
4. Wang, Y., Wang, X., Flueckiger, J., Yun, H., Shi, W., Bojko, R., Jaeger, N. A. F., Chrostowski, L. (2014). Focusing sub-wavelength grating couplers with low back reflections for rapid prototyping of silicon photonic circuits. Optics Express, 22, 20652–20662. https://doi.org/10.1364/oe.22.020652
5. Jalali, B., Fathpour, S. (2006). Silicon Photonics. Journal of Lightwave Technology, 24(12), 4600-4615. https://doi.org/10.1109/JLT.2006.885782
6. Saghaei, H., Elyasi, P., Karimzadeh, R. (2019). Design, fabrication, and characterization of Mach–Zehnder interferometers. Photonics Nanostructures: Fundamentals and Applications, 37, 100733. https://doi.org/10.1016/j.photonics.2019.100733
7. Rabus, D. G., Sada, C. (Springer Series in Optical Sciences, 127). Integrated Ring Resonators: A Compendium (2nd ed.). Springer.
8. Tai, H. (n.d.). Theory of Fiber Optical Bragg Grating - Revisited. Langley Research Center, NASA, Hampton, VA 23681.

9. Probestation, SiEPIC. (n.d.). `http://siepic.ubc.ca/probestation`, using Python code developed by Michael Caverley.
10. PLC Connections. (n.d.). `www.plcconnections.com`, PLC Connections, Columbus OH, USA.
11. Maple Leaf Photonics. (n.d.). `http://mapleleafphotonics.com`, Maple Leaf Photonics, Seattle WA, USA.